Electronic Supplementary Material (ESI) for RSC Advances.

Electronic Supplementary Information

Blue phase-mixed anatase-rutile TiO_2 heterogeneous junctions composites: surface defect-induced reconstruction by F ion and superior lithium-storage properties†

Hai Wang, Hongxing Yang* and Lin Lu

Renewable Energy Research Group (RERG), Department of Building Services Engineering, The Hong Kong Polytechnic University, Room: ZN816, Kowloon, Hong Kong, China. Fax: +852-27746146; Tel: +852-27665863; E-mail: bxhxyang@polyu.edu.hk.

Experimental section

Material synthesis

All chemical reagents were commercial products used without further purification. For the typical synthesis of anatase-rutile single crystal composites, 0.5 g of NaF was dissolved in 30 mL of deionized water-HCl mixed solution (volume ratio = 3 : 1) at room temperature. Then 0.5 g TiH_2 powder was added into the solution mentioned above with vigorous stirring for 10 min. The resulting suspension was then transferred to a Teflon-lined autoclave and heated at 180 °C for 14 h (denoted as ART). The as-prepared powders were collected by filtration and thoroughly washed with water and ethanol and finally dried in air at 70 °C. To explore the effects of the reaction conditions on the morphologies of final products, NaF, HCl and reaction time was accordingly changed while keeping other reaction conditions unchanged. To illustrate the role of interface in LIBs applications, the ART samples were obtained through a heat treatment process at 600 ℃ for 1 h (denoted as SART).

Material characterizations

X-Ray diffraction (XRD) data was collected from 20 to 80° 2θ counting for 2 s per step at room temperature on a PANanalytic X'Pert diffractometer (Cu-K_α radiation, λ = 0.15405 nm, voltage 40 kV, current 40 mA) with 1 fixed divergence and antiscatter slits and a 0.2 mm receiving slit. The surface morphologies of the samples were studied using a JEOL JSM6300 (Tokyo, Japan) field emission scanning electron microscope (FESEM). High-resolution transmission electron microscopy (HRTEM) images were obtained with a JEOL JEM-2010F microscope operating at 200 kV. The specific surface area and the pore size distribution (BJH method, desorption branch) were determined by nitrogen adsorption-desorption isotherms (Micromeritics, ASAP 2010), after evacuation at 200 °C for 12 h. The EPR spectra were recorded on a Bruker EMX EPR spectrometer at an X-band frequency of 9.363 GHz, sweep width of 500.00 Gauss, and center field of 3390.00 Gauss at 77K.

The weight content of anatase and rutile phase was calculated as follows:[1]

$$W_R = 1/[1+0.8(I_A/I_R)] \quad (1)$$

$$W_A = 1-W_R \quad (2)$$

where W_A and W_R are the weight fraction of anatase and rutile, I_A and I_R are the integrated intensities of s of anatase (101) and rutile (110), respectively.

The average crystalline sizes of anatase and rutile in the ART samples were obtained by employing the Debye-Scherrer formula on the anatase (101) and rutile (110) diffraction peaks.

Electrochemical measurements

The electrochemical measurements were carried out using CR2025-type coin cells with pure lithium metal as both the counter electrode and the reference electrode at room temperature. The working electrode consisted of active material, a conductive agent (carbon black, Super-P-Li), and a polymer binder (poly(vinylidene difluoride), PVDF, Aldrich) in a 70 : 20 : 10 weight ratio. The mass of active material in each electrode was about 1.5 mg. A Celgard 3400 membrane was used as a separator and 1.0 M $LiPF_6$ in a mixture of ethylene carbonate-diethyl carbonate (1 : 1 volume, Novolyte Technologies, USA) was used as the electrolyte. Cell assembly was carried out in an Ar-filled glovebox with concentrations of moisture and oxygen below 1.0 ppm. The charge-discharge cycling and cyclic voltammetry (CV) (1-3 V, 0.2 mV s^{-1}) was performed at room temperature using an electrochemical

workstation (CHI 860 D, Beijing) using a battery testing system (NEWARE) at different current rates with a voltage window of 1-3 V. Electrochemical impedance spectroscopy (EIS) measurements were performed at frequencies ranging from 10^{-2} to 10^{5} Hz. Reference experiments were performed by using SART as anode material.

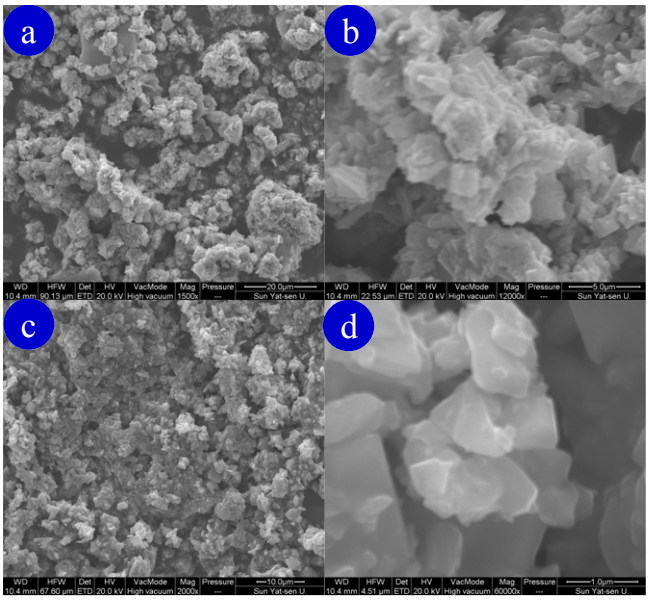

Fig.S1 The FESEM images of the samples at different contents of NaF.(a)-(b) 0.3 g; (c)-(d) 0.8 g.

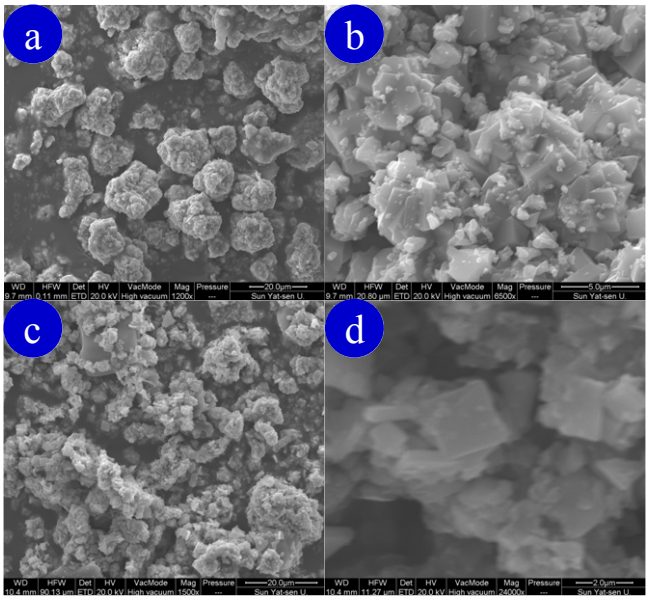

Fig.S2 The FESEM images of the samples at different volumes of HCl. (a)-(b) 5 ml; (c)-(d)15 ml.

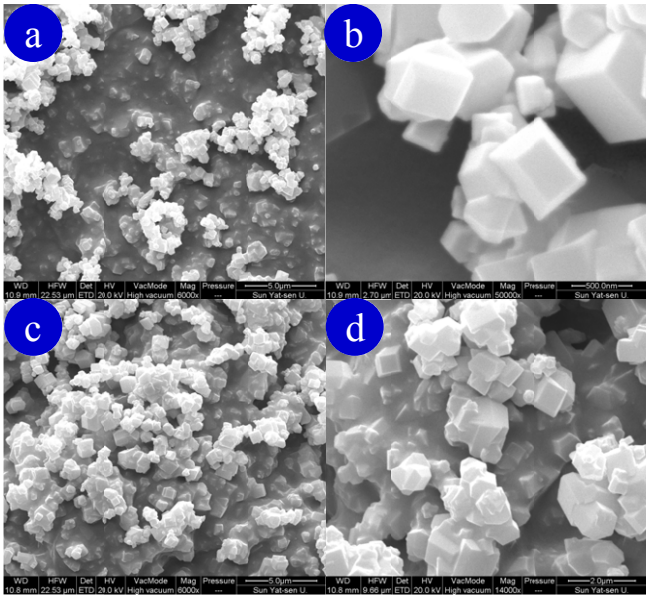

Fig.S3 The FESEM images of the samples at different reaction time. (a)-(b) 18 h; (c)-(d) 22 h.

Based on the microstructure comparison analysis of ART, obviously, the formation of ART is effected by the chemical reaction conditions. Another interesting problem arises: why is the obtained phase not a pure single phase, such as anatase, but mixed phases? There are two sides to address this problem. On one hand, previous experimental studies show that the anatase can be transferred into rutile when the surface defects exhibit under proper reaction conditions.[2-4] Therefore, the mixture phases are thus formed. On the other hand, the formation mechanism of formation of self-doping Ti^{3+} can be explained as follows: (i) TiH_2, as an intermetallic compound, plays a key role in the crystal growth of self-doped blue TiO_2. Oxidation is inevitable in the presence in the HCl and NaF solution under hydrothermal conditions; (ii) the F ion creates many opportunities for the formation of antase TiO_2 with exposed {001} facet; (iii) rutile-TiO_2 shells are induced to form on the surface of anatase-TiO_2 with exposed {001} facet due to the rich surface defects.

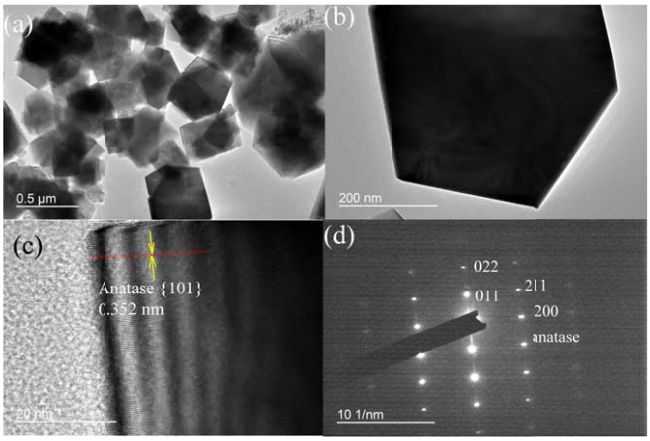

Fig. S4 TEM image of SART (a) and (b); HRTEM image of SART recorded from a single TiO_2 microcrystal (c) and the SAED patterns (d).

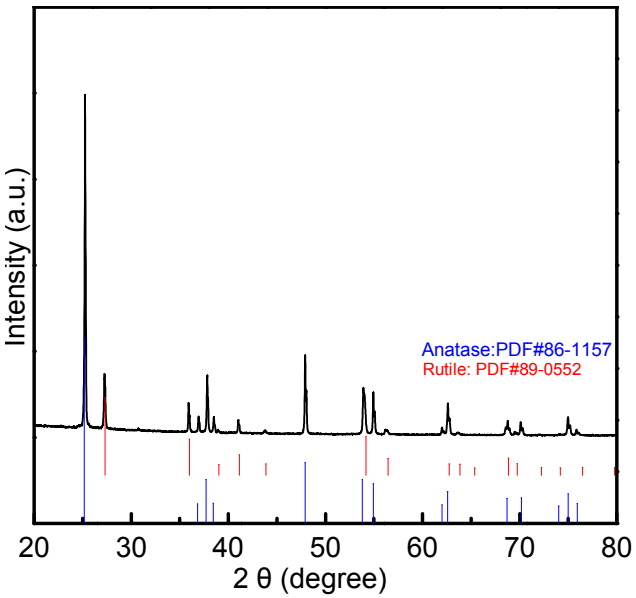

Fig. S5 XRD patterns of ART.

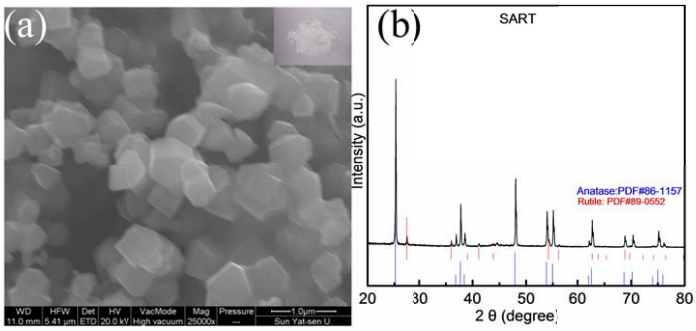

Fig. S6 The FESEM image of SART (a) and its XRD patterns (b).

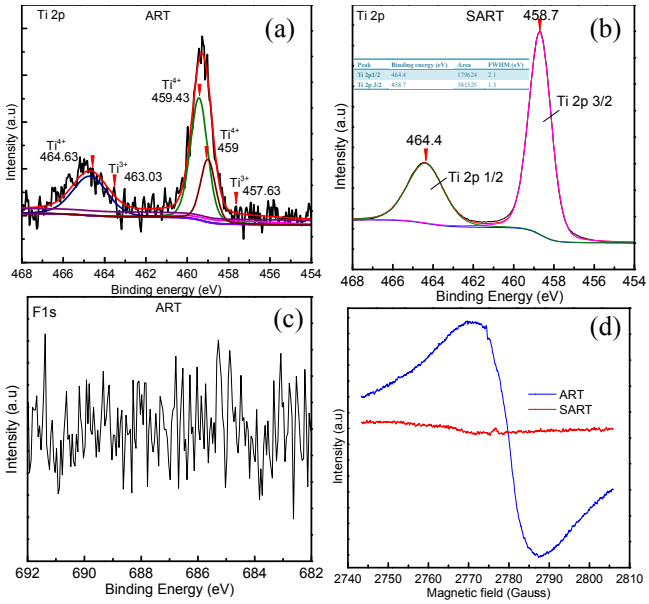

Fig. S7 High resolution XPS spectrum of Ti 2p core-level spectra of ART (a) and SART (b); (c) F 1s signal, demonstrating the lack of F residue; (d) EPR spectra of the ART and SART samples.

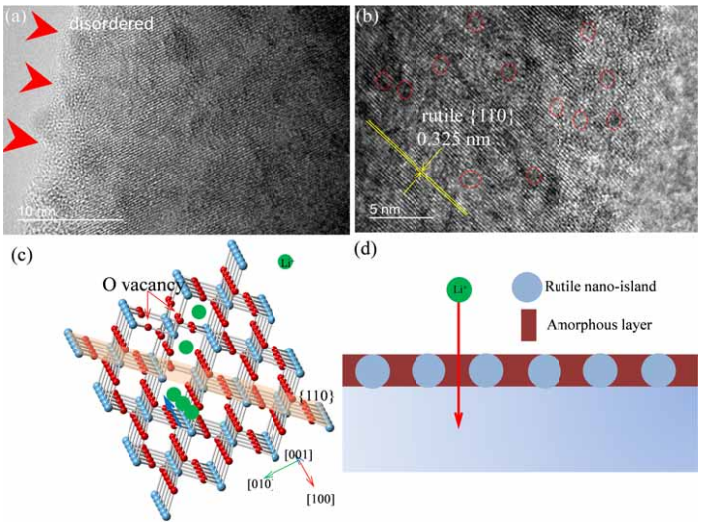

Fig. S8 The HRTEM images of a typical disordered layer. The rutile TiO_2 quantum dots are embedded in the disordered matrix (a)-(b). Note that the abundant defects marked by red circles and defects such as dislocations and distortions are clearly seen. Illustrations of the crystal structure and lithium ion insertion of the rutile (c) along the [001] projected directions. (d) lithium-ion transport across the interface of amorphous layer and rutile TiO_2 quantum dots.

The HRTEM technique was used to observe the surface structure of ART. The edges of the ART are very rough, with some distortion of lattice fringes including bending and dislocation, as shown in Fig.. S8a, which clearly reveals that a large number of defect sites was formed on the surface of ART. On the contrary, SART has a perfect crystalline structure with few visible defects (Fig. S4). In this case, the randomly distributed local defects are visible, as shown in Fig. S8b.

The significance of amorphous layer and rutile-TiO_2 quantum dots is that, on one hand, amorphous layer protects the liquid electrolyte from further decomposition, and blocks the direct contact of electrode and electrolyte, which is beneficial for the formation of stable SEI thin film and the transportation of lithium ion into the anatase. On the other hand, the rutile-TiO_2 quantum dots maximize the effective electrochemical utilization of the active materials.

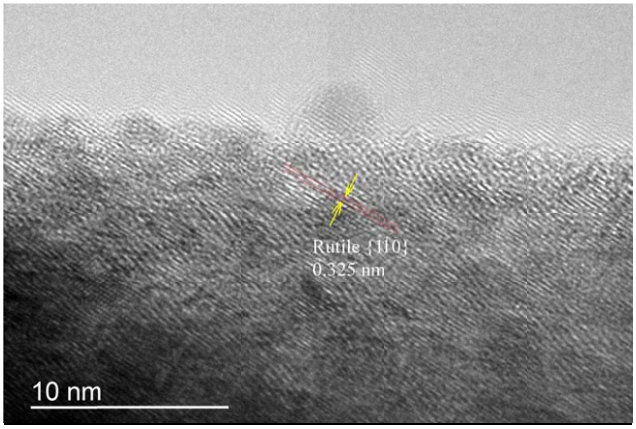

Fig. S9. A typical HRTEM image of rutile TiO_2 epitaxy layer of anatase TiO_2 {110} facets.

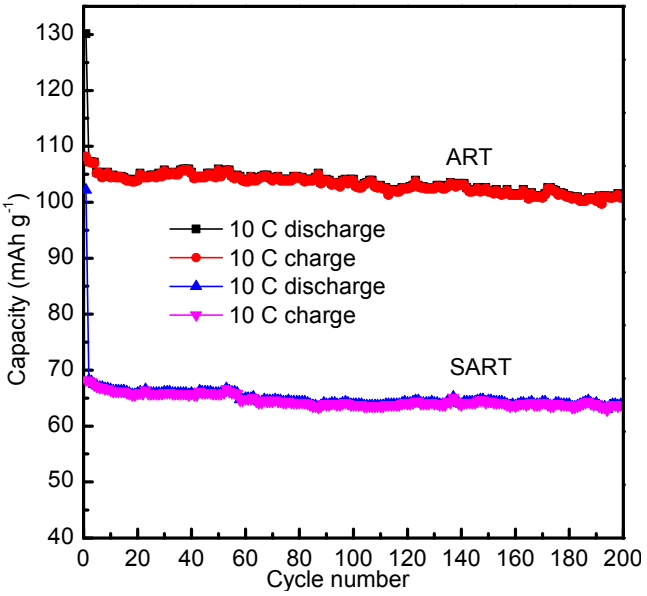

Fig. S10 Cycling performance of ART and SART electrodes at the rate of 10 C.

The surface area and pore-size distribution are two key factors for active materials in electrochemical reaction; therefore, the surface area and porosity of the as-prepared samples were investigated by nitrogen sorption measurement (Fig.S11). As shown in Fig. S11a, the isotherm of ART exhibits a typical microporous characteristic without distinct hysteresis. Nevertheless, SART exhibits a type IV isotherm as a result of the mesoporosity with an IUPAC type H3 hysteresis loop in the p/p_o range of 0.45-1.0 [5] (Fig. S11b). As listed in Tab 1, the specific surface areas of ART and SART were determined to be 10.11 and 4.77 $m^2 g^{-1}$, respectively. The decreased specific surface area of SART may be due to the mesoporous texture derived from the disappearance of the amorphous layer and rutile-TiO_2 quantum dots of ART. The micropores of ART mainly come from the interface of the amorphous layer with embedded rutile quantum dots.

The pore size distribution calculated from desorption data using the BJH model indicates that the pore size of the ART sample appears to be primarily 1.36 nm and 1.75 nm, respectively. It is reported that these porous structures can enhance the electrochemical activity by increasing the active sites of electrodes, which is favorable for the transport and diffusion of electrolyte ions during the charge-discharge process.

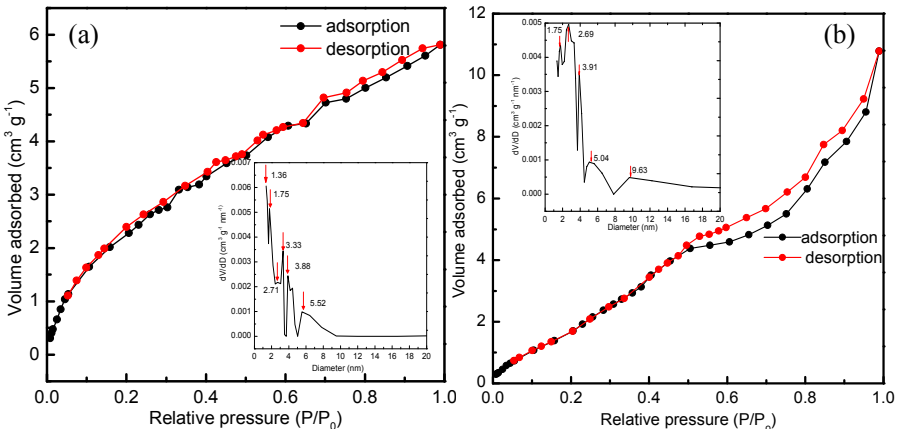

Fig. S11. Nitrogen adsorption and desorption isotherms and pore-size distribution curves (inset) of the ART (a) and SART (b) sample. According to BJH method, a maximum of the pore size distribution taken from the description branch.

Tab S1 Nitrogen physisorption parameters of ART and SART.

Samples	Surface area [a] ($m^2\ g^{-1}$)	Pore volume [b] ($cm^3\ g^{-1}$)	Average pore diameter [c] (nm)
ART	10.114	8.990×10^{-3}	3.55541 nm
SART	4.769	1.667×10^{-2}	13.9853 nm

[a]BET specific surface area calculated from the linear part of BET plot.

[b]Total pore volume taken from the volume of N_2 adsorbed at $p/p_0 = 0.98$.

[c]Average pore Radius was estimated from the Barrett-Joyner-Halenda formula.

Tab S2 Impedance parameters of the ART and SART electrodes calculated from the equivalent circuit.

Electrodes	R_s (Ω)	R_{ct} (Ω)
SART	14.5	138.4
ART	12.2	72.3

References:

1 H. Z. Zhang and J. F. Banfield, *J. Phys. Chem. B.*, 2000, **104**, 3481-3487.

2 F. C. Gennari and D. M. Pasquevich, *J. Mater. Sci.*, 1998, **33**, 1571-1578.

3 K. J. D. Mackenzie, *Brit. Ceram. Trans. J.*, 1975, **74**, 77-84.

4 E. F. Heald and C. W. Weiss, *Am. Mineral.*, 1972, **57**, 10-&.

5 J. M. Haynes, *J. Chem. Soc. Farad. T. 1*, 1983, **79**, 1059-1060.